Experimental Eye Research 209 (2021) 108641

Contents lists available at ScienceDirect

Experimental Eye Research

journal homepage: www.elsevier.com/locate/yexer

N-retinylidene-*N*-retinylethanolamine adduct induces expression of chronic inflammation cytokines in retinal pigment epithelium cells

Concetta Scimone [a,b], Luigi Donato [a,b,*], Simona Alibrandi [a,c], Maria Vadalà [d], Giuseppe Giglia [e], Antonina Sidoti [a], Rosalia D'Angelo [a]

[a] Department of Biomedical, Dental, Morphological and Functional Imaging Sciences, University of Messina, Via Consolare Valeria 1, 98125, Messina, Italy
[b] Department of Biomolecular Strategies, Genetics and Avant-Garde Therapies, I.E.ME.S.T., Via Michele Miraglia, 90139, Palermo, Italy
[c] Department of Chemical, Biological, Pharmaceutical and Environmental Sciences, University of Messina, Viale Ferdinando Stagno d'Alcontres 31, 98166, Messina, Italy
[d] Department of Experimental Biomedicine and Clinical Neuroscience, Ophthalmology Section, University of Palermo, 90127, Palermo, Italy
[e] Department of Biomedicine, Neuroscience and Advanced Diagnostics (BiND), Section of Human Physiology, University of Palermo, 90134, Palermo, Italy

ARTICLE INFO

Keywords:
A2E
Inflammation
RPE
Retinal degeneration
Oxidative stress
Expression analysis

ABSTRACT

Blindness due to photoreceptor degeneration is observed in both genetic and acquired eye disorders. Long blue light exposure can contribute to increase levels of oxidative compounds within the retinal pigment epithelium (RPE), enhancing risk of retinal damage. In retina, reactive oxygen species contribute to the activation of inflammatory cascade. If chronic, this inflammatory response can result in photoreceptor death. Therefore, we investigated the effects of the endogenous adduct *N*-retinylidene-*N*-retinylethanolamine (A2E) on RPE cells, in order to identify the most dysregulated cytokines and their related inflammatory pathways. RPE cells were exposed to A2E and blue light for 3h and 6h. By transcriptome analysis, we identified differentially expressed genes in A2E-treated cells, when compared to untreated ones. Expression values were quantified by the Limma R package. Enrichment analysis was performed according to the "Reactome" and the Gene Ontology databases. Expression of pro-inflammatory cytokines increased after 3h of A2E treatment and pathways related to IL-6 and IL-1 signaling resulted enriched. Also the up-regulation of genes having a protective role against inflammation was observed. Moreover, our results show that ferroptosis could contribute to RPE degeneration induced by A2E and blue light. Dysregulated genes related to retinal degeneration triggered by oxidative damage and inflammatory response activation identified in this study can be considered as potential biomarkers for targeted therapies.

1. Introduction

Retinal degeneration due to photoreceptor death is the cause of blindness usually observed in pathological eye conditions as age-related macular degeneration (AMD)1 (Somasundaran, 2020), Retinitis Pigmentosa (RP) and Stargardt disease (Strait, 2020). Several genetic and environmental factors contribute to retinal degeneration, and inflammation triggered by excessive reactive oxygen species (ROS) is a key event (Bermúdez, 2019). In retina, ROS imbalance can occur following light exposure damaging the retinal pigment epithelium (RPE) (Narimatsu, 2015). The RPE is the basal retinal monolayer made of polarized neural crista-derived pigmented epithelial cells. On the apical side, RPE interacts with the outer segments of the photoreceptors while, on the basolateral one, with the Bruch's membrane and the choriocapillaris. By separating photoreceptors from the choriocapillaris vascular bed, RPE provides nutrients for photoreceptors. Moreover, RPE contributes to maintain the negative hydrostatic pressure required for adhesion between the RPE and the photoreceptors (Kirchhof and Ryan, 1993) and is the site of chromophore renewal (Muñiz, 2014). Chromophore recycling reactions generate brown pigments called lipofuscins that can accumulate increasing risk of retinal degeneration. *N*-retinylidene-*N*-retinylethanolamine (A2E) is one of the most characterized fluorophores of RPE lipofuscin and it is synthetized from all-*trans*-retinal and phosphatidylethanolamine, following long light exposure. When exposed to blue light, A2E generates ROS, becoming toxic to RPE (Wang, 2018). The reduced defense of RPE against ROS due to the decreased antioxidant enzymatic activity can lead to the impairment of visual cycle

* Corresponding author. Department of Biomedical, Dental, Morphological and Functional Imaging Sciences, University of Messina, Via Consolare Valeria 1, 98125, Messina, Italy.
E-mail address: ldonato@unime.it (L. Donato).

https://doi.org/10.1016/j.exer.2021.108641
Received 7 November 2020; Received in revised form 6 May 2021; Accepted 24 May 2021
Available online 29 May 2021

Abbreviations

A2E	*N*-retinylidene-*N*-retinylethanolamine
AMD	age-related macular degeneration
FC	fold change
IL	interleukin
ROS	reactive oxygen species
RP	retinitis pigmentosa
RPE	retinal pigment epithelium

in A2E-treated RPE (Anderson, 2020). Moreover, 26 pro-inflammatory cytokines resulted upregulated after A2E exposure, in Human induced pluripotent stem cell-derived RPE (hiPSCs-RPE) (Parmar, 2018). In order to provide a wider description of inflammatory response triggered by A2E treatment in RPE cells (Alaimo, 2020), we evaluated expression of inflammatory markers by whole transcriptome analysis, considering two different time points since A2E exposure, in presence of blue light.

2. Materials and methods

2.1. Human Retinal Pigment Epithelial Cells culture, experimental conditions and viability assay

Table 1
Coding genes selected for validation by qRT-PCR. For each time point, the 3 most down-expressed and the 3 most up-regulated coding genes were selected. For each gene, the HUGO Gene Nomenclature Committee (HGNC) name, the Ensembl Gene and specific Transcript IDs, the $\log_2$ Fold Change detected by RNA-seq, the primer pair designed for qRT-PCR reactions and the specific length of the amplicon are reported.

Sample	HGNC Gene Name (ID)	Ensembl Gene ID	Ensembl Transcript ID	RNAseq $\log_2$ FC	Primer pair	Fragment length (bp)
RPE 3hvs0	*HMOX1* (5013)	ENSG00000100292	ENST00000216117.9	−2.192420772	F: ATTCTCTTGGCTGGCTTCCT R: TGTGCTTTTCGTTGGGGAAG	124
	SLC7A11 (11059)	ENSG00000151012	ENST00000280612.9	−2.067785858	F: CAAGGTGCCACTGTTCATCC R: GTGATGACGAAGCCAATCCC	108
	GCLM (4312)	ENSG00000023909	ENST00000370238.8	−2.062207345	F: AGCAACTACTGTCACCTCCA R: AGAGCCCACAGTATCCCAAC	128
	MVK (7530)	ENSG00000110921	ENST00000228510.8	2.035274371	F: AAGTGGACCTCAGCTTACCC R: TCTCCACTTGCTCTGAGGTG	126
	LDLR (6547)	ENSG00000130164	ENST00000558518.6	2.373452915	F: CGATGAAGTTGGCTGCGTTA R: GCAGTCTCTAGCCATGTTGC	112
	APOE (613)	ENSG00000130203	ENST00000252486.9	4.841387776	F: CTCAGCTCCCAGGTCACC R: GGGTCAGTTGTTCCTCCAGT	97
RPE 6hvs0	*IL11*RA (5967)	ENSG00000137070	ENST00000555003.5	−3.433289128	F: TTGGCCTCAGTGATTCCAGT R: ATCCACACCAGCAAGACAGA	108
	AKR1C3 (386)	ENSG00000196139	ENST00000380554.5	−3.075220122	F: GGAGGCCATGGAGAAGTGTA R: GCTTGTACTTGAGTCCTGGC	113
	IL1RN (6000)	ENSG00000136689	ENST00000361779.7	−2.856609992	F: AAGATGTGCCTGTCCTGTGT R: TCGCTCAGGTCAGTGATGTT	80
	TRIB2 (30809)	ENSG00000071575	ENST00000155926.8	2.303112678	F: TGCGATCCTCACACTCATGA R: AATCCTGGGTTTTGTTCCGC	86
	IL11 (5966)	ENSG00000095752	ENST00000264563.7	4.311356909	F: GACAAATTCCCAGCTGACGG R: CACACCTGGGAGCTGTAGAG	96
	ID1 (5360)	ENSG00000125968	ENST00000376105.4	4.936642208	F: GCTGTTACTCACGCCTCAAG R: CTCCAACTGAAGGTCCCTGA	113

Table 2
Noncoding genes selected for validation by qRT-PCR. Noncoding RNAs analyzed by the LncRRIsearch tool were selected for qRT-PCR validation. For each gene, the table shows the gene name, the Ensembl Gene and specific Transcript IDs, the $\log_2$ Fold Change detected by RNAseq at both time points, the primer pair designed for qRT-PCR reactions and the specific length of the amplified fragment.

Gene Name	Ensembl Gene ID	Ensembl Transcript ID	RNAseq $\log_2$ FC_3hvs0	RNAseq $\log_2$ FC_6hvs0	Primer pair	Fragment length (bp)
AC002094.1	ENSG00000258924	ENST00000591482.1	3.138743039	2.704183821	F: ACCTGGGAAAGCAAGTGAGA R: GGCTTCCAAGGTAAGTGCAG	102
AC099329.1	ENSG00000235288	ENST00000629885.1	2.944742883	2.661105865	F: GCACACCAAAGGCAAAGAGA R: ACTCTCAGTCTCAGCGTCTG	83
AC011611.3	ENSG00000257453	ENST00000552367.1	2.21614808	3.514449248	F: ATGTTGGAGAAGTGCAGTTC R: AGCAGCAGCAGCAACAACAG	118
AC135048.1	ENSG00000261487	ENST00000562642.1	2.372246758	2.022001098	F: CATGAAACTGAACTTGGACT R: GTGTTGAGATCAGATACCTT	109

and to photoreceptor apoptosis (Sun, 2018). Light-induced oxidative damage indeed is not limited to RPE cells but it also occurs in Müller cells and microglia, resulting in the activation of chemokine-mediated inflammation (Rutar, 2015). We previously highlighted the main dysregulated pathways in RPE, following A2E exposure and, among these, oxidative stress response pathways resulted highly enriched (Donato, 2020a). Here, we want to focus on inflammation response triggered by A2E treatment. Role of inflammasome in retinal degeneration was recently shown (Wooff, 2020) as well as the increased IL-1β production

Human RPE-derived primary Cells at the 2nd passage (H-RPE - Human Retinal Pigment Epithelial Cells, Clonetics™, Lonza, Walkersville, USA) were grown, as previously described (Donato, 2020b), in T-75 flasks with RtEGM™ Retinal Pigment Epithelial Cell Growth Medium BulletKit® (Clonetics™, Lonza, Walkersville, MD, USA), supplied with 2% v/v fetal bovine serum (FBS), 1% of penicillin/streptomycin and incubated at 37 °C with 5% CO_2. 96-well plates were used to plate 4 × 10^4 cells/well. When confluent, H-RPE were treated with 20 μM A2E. A2E cytotoxicity was induced by irradiating H-RPE cells with blue light.

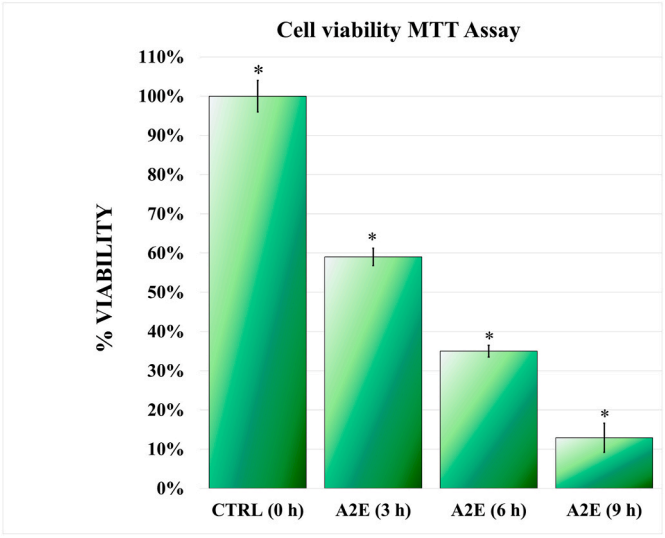

Fig. 1. MTT assay results. Cytotoxic effects of *N*-retinylidene-*N*-retinylethanolamine (A2E) on retinal pigment epithelium (H-RPE) cells increases in a time-dependent manner. Viability of untreated (0h) H-RPE cells, 3h, 6h and 9h A2E exposed H-RPE cells is expressed in percentage, as mean ± SD (n = 3). Due to the low viability rate, H-RPE cells after 9h of A2E treatment were excluded from the analysis. (*): pValue < 0.05, calculated by the multiple *t*-test.

In detail, cultures were transferred to Phosphate Buffered Saline (PBS) supplemented with calcium, magnesium and glucose (PBS–CMG) and exposed to a tungsten-halogen source (470 ± 20 nm; 0.4 mW/mm2) for 30 min. Cells were incubated at 37 °C. After treatment, three different time points, 3h, 6h and 9h, were considered. As negative control, untreated H-RPE cells were maintained at the same conditions, exoposed to the blue light and without A2E treatment. Following A2E treatment, RPE cells viability was assessed by the mitochondrial-dependent reduction of methylthiazolyldiphenyl-tetrazolium bromide (MTT) (Sigma-Aldrich, St. Louis, MO, USA) to formazan insoluble crystals assay, as previously reported (Donato, 2020b). In detail, 10 μL of 5 mg/mL of MTT were diluted in PBS and added to the cell medium. Cultures were incubated for 2h at 37 °C and, then, 100 μL of 10% SDS in 0.01 mol/L HCl were added. Following this treatment, cells were incubated for 16h, before being read in a Dynatech microplate reader. The 570 nm absorbance was set. Viability of A2E treated cells was normalized against the negative control one. Three biological replicates were realized.

2.2. RNA extraction and whole transcriptome analysis

Total RNA was purified by TRIzol™ Reagent (Invitrogen™, ThermoFisher Scientific, Waltham, MA, USA), as already described following manufacturer's protocol (Donato, 2020b). Quantification was performed by the Qubit 2.0 fluorimeter and the Qubit® RNA assay kit (InvitrogenTM, ThermoFisher Scientific, Waltham, MA, USA). RNA was extracted before A2E treatment (time point: 0h - negative control), and following both 3h and 6h of the A2E exposure. Each time point was three times processed. Therefore, nine libraries were totally generated. In detail, paired-end libraries were obtained using 1 μg of total RNA, by the TruSeq Stranded Total RNA Sample Prep Kit with Ribo-Zero H/M/R (Illumina, San Diego, CA, USA). Amplified libraries were run on a HiSeq 2500 Sequencer (Illumina, San Diego, CA, USA), using the HiSeq SBS Kit v4 (Illumina, San Diego, CA, USA).

2.3. FASTQ data quality control and read mapping

Raw data generated by the paired-end libraries sequencing were processed as previously reported (Donato, 2020b). Quality check was performed by the FastQC (v.0.11.9) (https://www.bioinformatics.babraham.ac.uk/projects/fastqc/) and the QualiMap (v.2.2.1) (Okonechnikov, 2016). Low quality reads (Phred score < 30) were removed by the Trimmomatic (v.0.39) tool (Bolger, 2014). Filtered reads were mapped to the GRCh38 Human Reference Genome and the Ensembl RNA database v.99, by the Qiagen CLC Genomics Workbench v.20.0 software package (Qiagen, Hilden, Germany) (https://digitalinsights.qiagen.com/products-overview/analysis-and-visualization/qiagen-clc-genomics-workbench/).

2.4. Gene expression quantification, differential gene expression (DGE) and statistical analysis

Following alignment, reads were quantified by the mapping-dependent expectation-maximization (EM) algorithm (Li, 2010). The Limma R package (Ritchie, 2015) was used to identify differentially expressed genes among three different conditions: i) untreated (0h) vs 3h_treated, ii) untreated (0h) vs 6h_treated, iii) 6h_treated vs 3h_treated. Differential expression was reported as $\log_2$ fold change ($\log_2$ FC) of the gene abundance. Statistical significance was assessed by the *t*-test. The Bonferroni-adjusted p-value < 0.05 was considered as significance threshold. Differentially expressed genes showing $\log_2$ FC < −2 and $\log_2$ FC > 2, for down- and up-regulated respectively, were considered for downstream analysis.

2.5. Functional gene annotation and enrichment analysis

Differentially expressed genes were annotated based on the InterPro (Mitchell, 2019), Reactome (Jassal, 2020), Human Protein Atlas (Uhlen, 2017), UniProt (The UniProt Consortium, 2018), IntAct (Orchard, 2014), Ensembl (Aken, 2016) and HGNC (Wain, 2002) databases. Functional enrichment analysis was performed by the ClueGo plug-in (Bindea, 2009) of the Cytoscape platform. DEGs were clustered

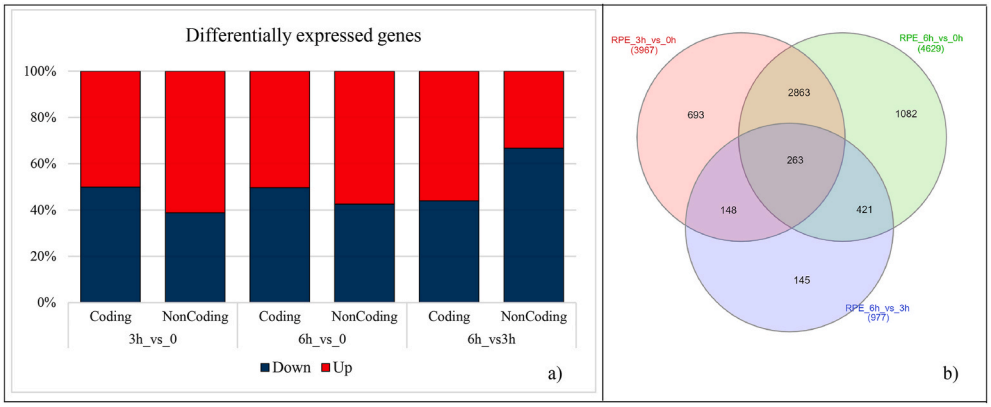

Fig. 2. Differentially Expressed Genes (DEGs) in A2E-treated RPE cells. a) The bar chart shows the percentage of DEGs detected in RPE cells treated with A2E when compared to untreated cultures. Blue portions refer to down-expressed genes, while red ones indicate the up-regulated ones. b) The Venn diagram (http://www.interactivenn.net/, Heberle, 2015) highlights dysregulated genes shared by the A2E-treated RPE cells, at the different time points considered (intersections). Details about outputted data are available in supplementary materials (SM4). (For interpretation of the references to colour in this figure legend, the reader is referred to the Web version of this article.)

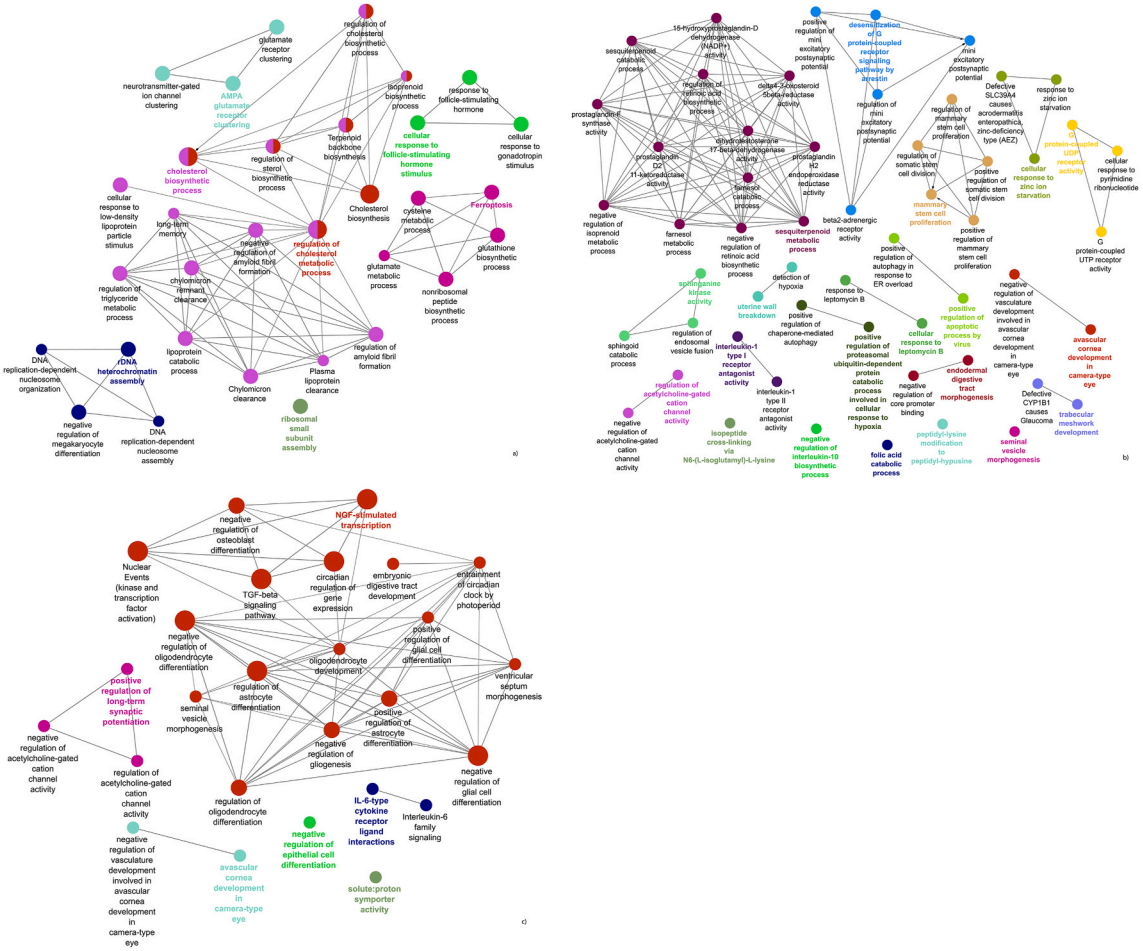

Fig. 3. Enrichment analysis results by the ClueGo tool. a) Functional enrichment results of DEGs in RPE cells 3h after A2E treatment (a), 6h after A2E treatment (b), and comparison between 6h and 3h after A2E treatment (c).

according to the "Gene Ontology (GO): Biological process" (The Gene Ontology Consortium, 2017), the Kyoto Encyclopedia of Genes and Genome (KEGG) (Kanehisa, 2017), Reactome (Jassal, 2020) and CORUM 3.0 (Giurgiu, 2019) annotation terms. In order to obtain more detailed results, GO Tree interval was set as Min Level = 6 and Max Level = 15, while the GO Term/Pathway Network Connectivity (Kappa Score) considered was 0.4. Only results showing a Bonferroni step-down pValue <0.05 were considered.

2.6. Identification of noncoding RNAs and target prediction

Differentially expressed genes mapping noncoding RNAs were outputted applying the above mentioned bioinformatic analysis pipeline, using the proper non-coding references. Before to proceed with down-stream analysis, differentially expressed genes were selected according to the following threshold values: $\log_2 FC < -2$ and $\log_2 FC > 2$ for down- and up-regulated genes, respectively. Statistical significance was attributed by considering the Bonferroni-adjusted p-value < 0.05. Targets of noncoding RNAs were predicted by the LncRRIsearch web tool (http://rtools.cbrc.jp/LncRRIsearch/index.cgi) (Fukunaga, 2019). This server predicts RNA - long noncoding RNA (lncRNA) interaction based on free energy, tissue-specific expression and subcellular localization data. Enrichment analysis of lncRNA target genes were performed by the Reactome pathway database (Jassal, 2020).

2.7. Quantitative RT-PCR data validation

Transcriptome data were validated by quantitative Real Time-Polymerase Chain Reaction (qRT-PCR). At each time point, 6 dysregulated coding genes (Table 1) and 4 dysregulated noncoding genes (Table 2) were selected for retrotranscription by the High-Capacity cDNA Reverse Transcription Kit with RNase Inhibitor (Applied Biosystems™, Fisher Scientific, Loughborough, Leicestershire, UK). In detail, 1 μg RNA was used for 20 μL of total reaction volume, according to manufacturer protocol. For the qRT-PCR reaction mix, 50 ng of cDNA, 200 nM of each specific primer and 10 μL SYBR™ Select Master Mix (Applied Biosystems™, Fisher Scientific, Loughborough, Leicestershire, UK) were mixed and run on an Applied Biosystems® 7500 Fast Real-Time PCR System (Applied Biosystems, Foster, USA). Each reaction was trice repeated. The average threshold cycle (Ct) was calculated by the values obtained for each reaction. Relative gene expression was quantified by the $2^{-\Delta\Delta Ct}$ method normalized versus the expression level of the β-actin. The IBM SPSS 26.0 software (https://www.ibm.com/analytics/us/en/technology/spss/) was used for linear regression analysis, in order to calculate correlation of fold change between qRT-PCR and RNA-Seq gene expression ratio.

2.8. Protein extraction and enzyme-linked immunosorbent assay (ELISA)

Proteins were purified from both untreated, 3h and 6h A2E-treated HRPE cells. In detail, cells were incubated with 1X Radioimmunoprecipitation assay buffer (RIPA) buffer, supplied with protease inhibitor mix.

The enzyme-linked immunosorbent assay (ELISA) was performed in order to quantify the Heme Oxygenase (HMOX1), the Cystine/glutamate transporter (SLC7A11) and the Glutamate Cysteine Ligase, Modifier

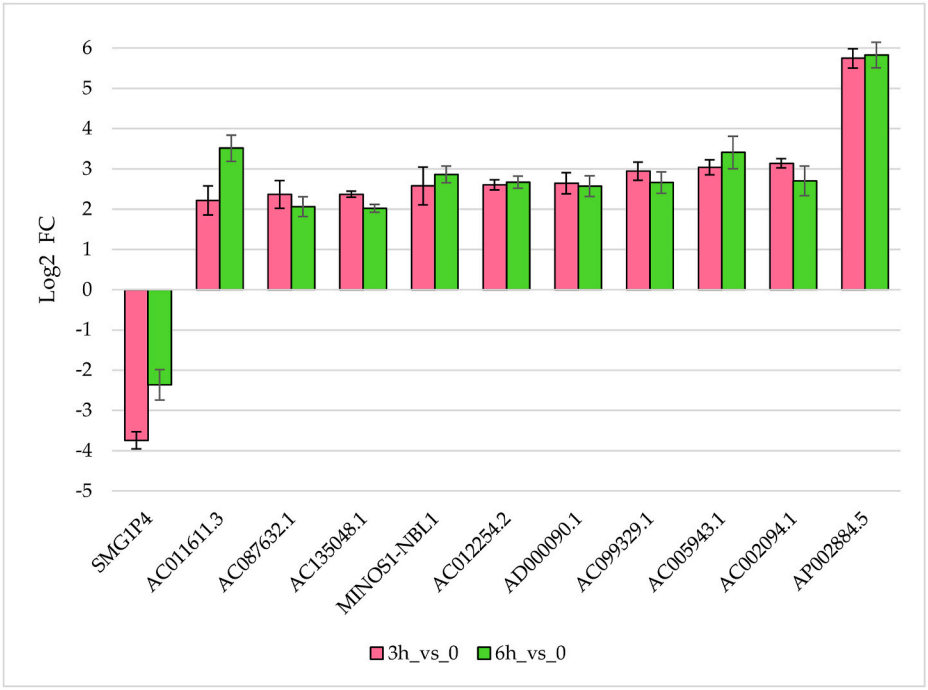

Fig. 4. Noncoding RNAs expression values. The histogram reports expression values, as $\log_2$ FC, of the long noncoding RNAs dysregulated at both time points (3h vs 0, pink bars; 6h vs 0, green bars). Reported values refer to the mean of the three biological replicates. Standard deviation is also indicated. (For interpretation of the references to colour in this figure legend, the reader is referred to the Web version of this article.)

Subunit (GCLM) proteins, as ferroptosis biomarkers. The GCLM and SLC7A11 ELISA Kits (MyBioSource, San Diego, SC, USA) and the HMOX1 DuoSet IC ELISA (R&D Systems, Bio-Techne, Minneapolis, MN, USA) were used to perform sandwich ELISA, according to manufacturer protocols. Protein samples were diluted (dilution factor 1/1000) and, for each time point, three replicas were considered. Plates were read by a microplate reader and protein quantification was assessed by comparison with the standard curves.

3. Results

3.1. Cell viability, transcriptome analysis and differential gene expression

The MTT assay performed on both A2E untreated and treated H-RPE cells showed that A2E had cytotoxic effect when activated by blue light irradiation and this cytotoxicity increased in a time-dependent manner. In detail, cell viability sensitively decreased after 9h of A2E treatment. For this reason, this time point was not considered for downstream analysis (Fig. 1).

Whole transcriptome sequencing approximatively generated 100,000,000 reads showing a mean mapping quality Phred score $\geq$30. Of these, 67.8% were uniquely mapped reads. By DGE analysis, 3967 genes resulted dysregulated at the first time point (3h) after the treatment, when compared to the untreated cells. This number increased up to 4629 at the second time point (6h). Finally, 977 genes resulted further dysregulated at the second time point following A2E treatment (6h), when compared to the first one (3h) (Fig. 2) (Supplementary Materials SM1 - sheet 1).

3.2. A2E treatment leads to early activation of lipid biosynthesis

Three hours after A2E treatment, functional annotation of most dysregulated genes revealed the enrichment of pathways related to lipid metabolism (Fig. 3a) (SM2 - sheet 1). Totally, 34 coding genes (SM1 - sheet 2) were filtered and clustered. In detail, genes involved in biosynthesis and transport of cholesterol (*MVK*, *APOE*, *LDLR*, *HMGCS1*) resulted up-regulated. Surprisingly, *GCLM*, encoding for the first-rate limiting enzyme of glutathione synthesis, was down-expressed together with *HMOX1* and *SLC7A11*. These genes were clustered in the same KEGG pathway (KEGG:04216 "Ferroptosis"). Ferroptosis is a regulated form of cell death characterized by the production of reactive oxygen species (ROS), accumulation of iron and lipid peroxidation and it can be induced by both endogenous compounds and xenobiotics (Bogdan, 2016). Expression of inflammation markers did not show significative change within 3 h of treatment.

3.3. Inflammatory response is later event in A2E-treated RPE cells

The number of dysregulated coding genes in RPE cells highly increased 6h after A2E treatment (SM1 - sheet 3): 113 genes were annotated to terms related to autophagy (GO:1904716, GO:0034263), apoptosis (GO:0060139, GO:0046521), response to hypoxia (GO:2000777), cell proliferation and division (GO:0002174), zinc ion homeostasis (GO:0034224), neurotransmitter metabolism (GO:1903048, GO:0002032) and retinoic acid biosynthesis (GO:1900052) (Fig. 3b) (SM2 - sheet 2). Moreover, inflammatory markers were detectable 6h after A2E treatment. In detail, expression of *IL11* was enormously increased ($\log_2$ FC = 4.3) when compared to untreated RPE cells. Another up-regulated gene was *TRIB2* ($\log_2$ FC = 2.3), clustered to the "negative regulation of interleukin-10 biosynthetic process" ontology (GO:0045081). Protection against inflammation stimuli was further weakened by decreased expression of *IL1RN* ($\log_2$ FC = −2.86), annotated to the "interleukin-1 receptor antagonist" terms (GO:0045352, GO:0045353). Finally, also *AKR1C3* resulted down-regulated ($\log_2$ FC = −3.07). It is involved in prostaglandin oxidoreductase activity (GO:0047017, GO:0036130, GO:0036131).

Considering the three time lapses, comparison of gene expression levels measured between the first time point following A2E treatment (3h vs 0) and the second one (6h vs 3h) revealed significative dysregulation of *IL11*RA ($\log_2$ FC = −3.4) and for *IL11* ($\log_2$ FC = 3.7) (SM1 - sheet 3). Both genes were clustered in pathways relate to IL-6 signaling (R-HSA:6783589 and R-HSA:6788467), suggesting that inflammatory

Table 3

Reactome annotation terms for genes targeted by dysregulated noncoding RNAs. Target genes of the long noncoding RNAs dysregulated in RPE cells after A2E treatment were functionally clustered according to the Reactome pathway database. For each pathway, the Reactome pathway identifier, the pathway name, the False Discovery Rate (FDR) – adjusted pValue and the clustered genes are reported.

Pathway identifier	Pathway name	Entities FDR	Submitted entities found
R-HSA-5673001	RAF/MAP kinase cascade	1.63024E+15	*CNKSR2;SYNGAP1;RAP1A;ERBB3;IRS1;NRG2;DUSP6*
R-HSA-9607240	FLT3 Signalling	1.63024E+15	*CNKSR2;SYNGAP1;RAP1A;ERBB3;IRS1;NRG2;DUSP6*
R-HSA-168256	Immune System	1.97214E+15	*MEF2A;FBXW4;TRIM41;PIANP;TNFRSF13B;IRS1;FBXL19;PLD4;NRG2;SRP14;DUSP6; IL18BP;CNKSR2;PPP3CA;SYNGAP1;RAP1A;ERBB3;FTH1;AP1S3;PRKACA*
R-HSA-392517	Rap1 signalling	2.74338E+16	*RAP1A;PRKACA*
R-HSA-1280215	Cytokine Signalling in Immune system	1.26785E+15	*CNKSR2;MEF2A;SYNGAP1;RAP1A;ERBB3;TNFRSF13B;IRS1;NRG2;PRKACA;DUSP6; IL18BP*
R-HSA-5621575	CD209 (DC-SIGN) signalling	2.61256E+16	*PRKACA*
R-HSA-1280218	Adaptive Immune System	2.62288E+16	*FBXW4;PPP3CA;PIANP;TRIM41;RAP1A;FBXL19;AP1S3;PRKACA*
R-HSA-5675221	Negative regulation of MAPK pathway	4.26083E+15	*DUSP6*
R-HSA-5674135	MAP2K and MAPK activation	5.90257E+15	*CNKSR2;RAP1A*
R-HSA-448424	Interleukin-17 signalling	5.90257E+15	*MEF2A;DUSP6*
R-HSA-168249	Innate Immune System	6.04825E+15	*MEF2A;PPP3CA;RAP1A;FTH1;PLD4;SRP14;PRKACA;DUSP6*
R-HSA-5621481	C-type lectin receptors (CLRs)	6.08663E+16	*PPP3CA;PRKACA*
R-HSA-9012546	Interleukin-18 signalling	6.15174E+16	*IL18BP*
R-HSA-975871	MyD88 cascade initiated on plasma membrane	6.15174E+16	*MEF2A;DUSP6*
R-HSA-168142	Toll Like Receptor 10 (TLR10) Cascade	6.15174E+16	*MEF2A;DUSP6*
R-HSA-168176	Toll Like Receptor 5 (TLR5) Cascade	6.15174E+16	*MEF2A;DUSP6*
R-HSA-2025928	Calcineurin activates NFAT	6.15174E+16	*PPP3CA*
R-HSA-975138	TRAF6 mediated induction of NFkB and MAP kinases upon TLR7/8 or 9 activation	6.15174E+16	*MEF2A;DUSP6*
R-HSA-168164	Toll Like Receptor 3 (TLR3) Cascade	6.15174E+16	*MEF2A;DUSP6*
R-HSA-975155	MyD88 dependent cascade initiated on endosome	6.15174E+16	*MEF2A;DUSP6*
R-HSA-168181	Toll Like Receptor 7/8 (TLR7/8) Cascade	6.15174E+16	*MEF2A;DUSP6*
R-HSA-937061	TRIF(TICAM1)-mediated TLR4 signalling	6.15174E+16	*MEF2A;DUSP6*
R-HSA-166166	MyD88-independent TLR4 cascade	6.15174E+16	*MEF2A;DUSP6*
R-HSA-168138	Toll Like Receptor 9 (TLR9) Cascade	6.15174E+16	*MEF2A;DUSP6*
R-HSA-166058	MyD88:MAL(TIRAP) cascade initiated on plasma membrane	6.15174E+16	*MEF2A;DUSP6*
R-HSA-168188	Toll Like Receptor TLR6:TLR2 Cascade	6.15174E+16	*MEF2A;DUSP6*
R-HSA-168179	Toll Like Receptor TLR1:TLR2 Cascade	6.15174E+16	*MEF2A;DUSP6*
R-HSA-181438	Toll Like Receptor 2 (TLR2) Cascade	6.15174E+16	*MEF2A;DUSP6*
R-HSA-449147	Signalling by Interleukins	6.15174E+16	*MEF2A;IRS1;PRKACA;DUSP6;IL18BP*
R-HSA-9664323	FCGR3A-mediated IL10 synthesis	8.07434E+15	*PRKACA*
R-HSA-1266695	Interleukin-7 signalling	9.84439E+15	*IRS1*
R-HSA-9008059	Interleukin-37 signalling	1.13406E+15	*IL18BP*
R-HSA-168898	Toll-like Receptor Cascades	1.25868E+16	*MEF2A;DUSP6*
R-HSA-512988	Interleukin-3, Interleukin-5 and GM-CSF signalling	1.54019E+15	*PRKACA*
R-HSA-1168372	Downstream signalling events of B Cell Receptor (BCR)	2.67695E+15	*PPP3CA*
	Interleukin-1 family signalling	4.21536E+16	*IL18BP*

(*continued on next page*)

Table 3 (*continued*)

Pathway identifier	Pathway name	Entities FDR	Submitted entities found
R-HSA-446652			
R-HSA-2029480	Fc-gamma receptor (FCGR) dependent phagocytosis	4.77324E+16	*PLD4*

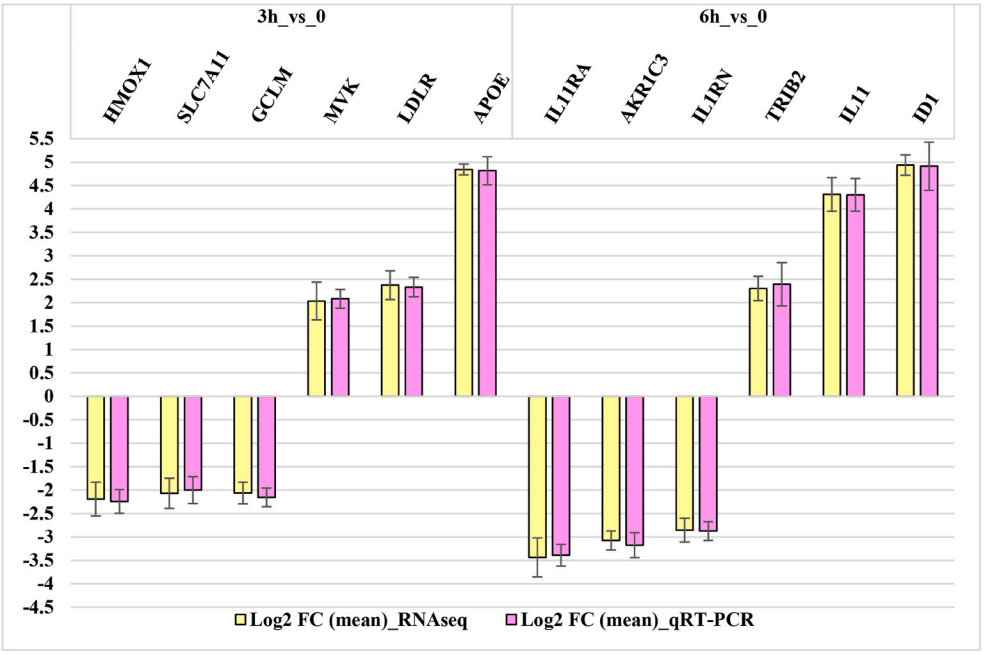

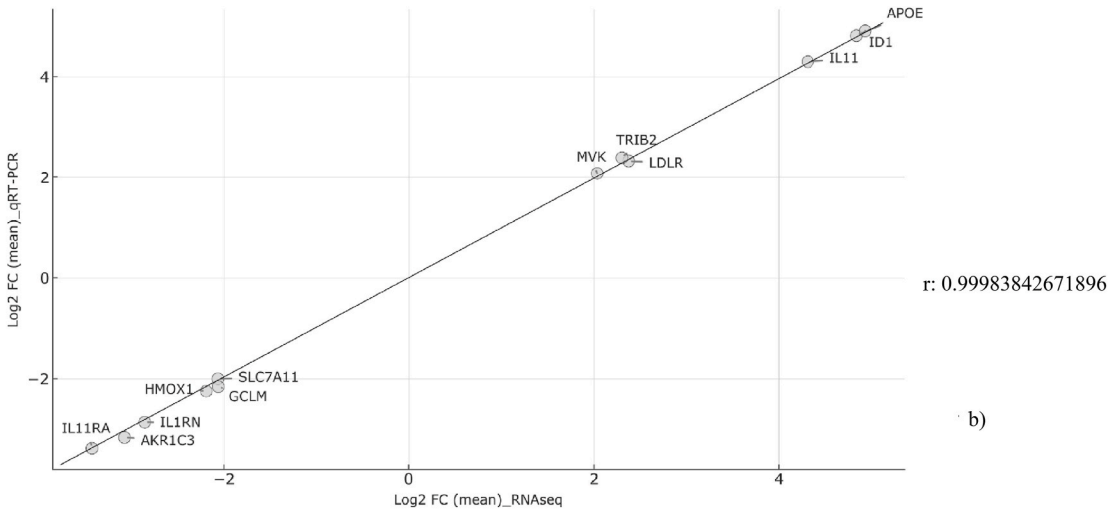

Fig. 5. Quantitative RT-PCR results – coding genes. a) Bar chart showing comparison between $\log_2$ FC values observed by qRT-PCR and RNA-seq of the dysregulated genes mentioned in the text, for each time point. In detail, for each sample 3 down-expressed and 3 up-regulated genes were considered. Represented values are the average values of the three replicates. Standard deviation is also indicated. b) Correlation analysis between $\log_2$ FC observed values by RNA-seq (*x*-axis) and qRT-PCR (*y*-axis) confirms reliability of RNA-seq data (r = 0.99983842671896).

response activation is triggered after 3 h of A2E treatment (Fig. 3c) (SM2 - sheets 2 and 3).

3.4. Noncoding RNA dysregulation and inflammasome

About noncoding RNAs, 85 and 101 transcripts resulted dysregulated 3h and 6h after the treatment, respectively (Fig. 2). Of these, 23 and 27 were selected according to filtering criteria (SM1 - sheets 4 and 5). Eleven noncoding RNAs were common to both time points, following the same trend (Fig. 4).

Of these, only 4 were found by the LncRRIsearch server (AC011611.3, AC135048.1, AC099329.1, AC002094.1) (SM3 - sheets 1–4). Reactome pathway analysis of annotated lncRNA targets highlighted the enrichment of pathways related to inflammation (SM3 - sheet

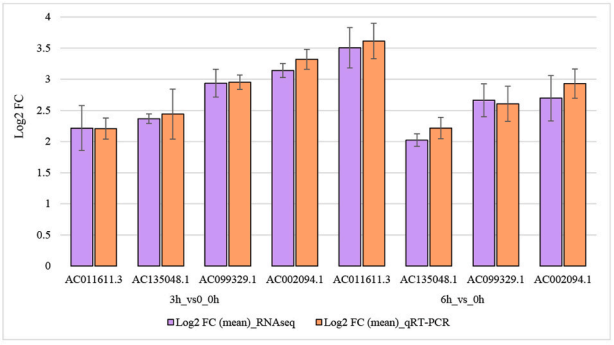

a)

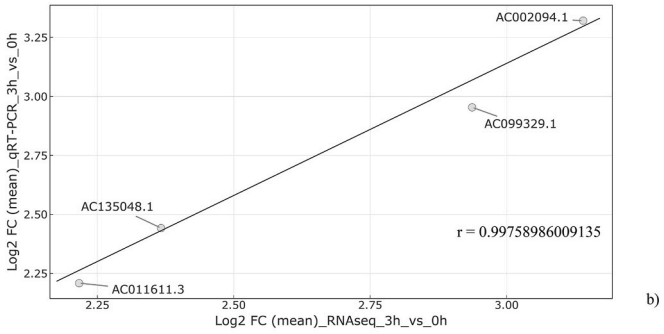

b)

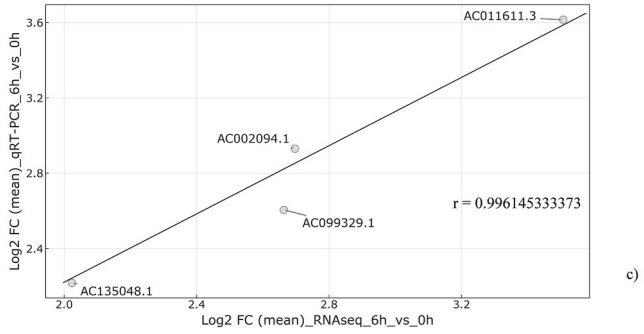

c)

Fig. 6. Quantitative RT-PCR results – noncoding genes. a) Bar chart showing comparison between log2 FC values observed by qRT-PCR and RNA-seq of the 4 noncoding genes enriched by the LncRRIsearch tool. The four transcripts were considered at both time points. Represented values are the average values of the three replicates. Standard deviation is also indicated. b-c) Correlation analysis between log_2 FC observed values by RNA-seq (*x*-axis) and qRT-PCR (y-axis) confirms reliability of RNA-seq data at both 3h (b) and 6h (c) after A23 treatment.

5) and, in particular to the signaling of IL-17 and Toll-like Receptors (*MEF2A*; *DUSP6*), IL-1, IL-18 and IL-37 (*IL18BP*), IL-10, IL-3 and IL-5 (*PRKACA*), calcineurin – NFAT cascade (*PPP3CA*) and IL-7 (*IRS1*), suggesting that A2E treatment can trigger mechanisms related to chronic inflammation (Table 3).

3.5. Quantitative real-time-PCR results

Expression values obtained by RNA sequencing were confirmed by qRT-PCR. Data are reported as the average of the three replicates. About coding transcripts, comparison of log_2 FC values between RNA-sequencing and qRT-PCR data are shown in Fig. 5a. According to the most enriched pathways, different genes were considered for the two time points. No significant differences were assessed between RNA-seq and qRT-PCR expression values, as confirmed by correlation analysis (Fig. 5b). Expression of four non-coding transcripts was, instead, considered at both 3h and 6h following A2E treatment (Fig. 6a). Also in this case, comparison of RNA-seq and qRT-PCR expression values confirmed transcriptome data reliability, despite correlation analysis showed greater dispersion (Fig. 6b).

3.6. 3.6. Quantitative determination of ferroptosis-related proteins by ELISA assay

In order to confirm proportion between gene expression level and protein quantity, HMOX1, SCL7A11 and GCLM were selected for data validation by ELISA assay. This choice was made being these proteins involved in ferroptosis enhancement. According to gene expression values, also protein quantities decreased in HRPE cells, following A2E exposure (Fig. 7). Reduced protein concentrations are also reported as linear regression, by plotting absorbance expressed as optical density (O. D.) (*y*-axis) against the protein concentration (*x*-axis).

4. Discussion

Retinal degeneration due to increased ROS level is the main cause of AMD occurring in adults. ROS impairment can also contribute to RP onset. Damage is mostly related to the high oxidative metabolism rate within retinal cells and, in particular, in RPE. Lipid oxidization normally occurs in retina as consequence of the visual cycle reactions. However, light exposure enhances biosynthesis of lipid adducts as A2E. Retinal degeneration linked to A2E exposure needs more clarification. In this context, we performed whole transcriptome analysis on H-RPE cells treated with A2E, focusing on degeneration mechanisms driven by the inflammatory cascade. In detail, no evidence of inflammatory response were observed within 3h after the treatment. In contrast, genes related to lipid biosynthesis and transport were upregulated, while genes involved in oxidative stress defense resulted down-regulated. Moreover, for the first time, we showed aberrant expression of genes involved in ferroptosis regulation, suggesting that this death mechanism could occur in A2E-treated H-RPE cells. Ferroptosis is an iron-dependent, non-apoptotic form of regulated cell death and it was shown in RPE, following inhibition of glutathione peroxidase 4 (Lee, 2020). A2E treatment caused the down-expression of *GCLM*, resulting in decreased biosynthesis of the glutathione. Together with *GCLM*, the ClueGo plugin clustered *SLC7A11* and *HMOX1* in the ferroptosis pathway (KEGG:04216). In detail, *SLC7A11* is required for cysteine entry within the cell while *HMOX1* is involved in iron homeostasis maintenance. Therefore, their down-expression and the subsequent reduced protein production potentially decrease levels of glutathione synthesized within the cell and impairs iron balance, inducing ferroptotic pathway (Kuang, 2020). Inflammation signature appeared within 6h of treatment. Human RPE cells do not constitutively express *IL11*, that has anti-apoptotic and anti-inflammatory functions (Nagineni, 2010). However, our results showed that its expression is enhanced by A2E, suggesting that this dysregulation can represent an attempt of survival in response to damaging compounds. On the other hand, excessive IL-11 levels can result in pathological phenotype due to the STAT3/AKT signaling activation (Zhao M, 2018; Zhuang, 2019). Notably, expression of the IL11 receptor-α (*IL11*RA) decreased, and this could lead to the loss of feedback mechanism, resulting in *IL11* upregulation. Also *IL1RN*, encoding for the Interleukin 1 Receptor Antagonist that inhibits proinflammatory activity of IL1 cytokine family members, resulted down-expressed. Moreover, inflammation is also enhanced by the increased expression of *TRIB2*, acting as repressor of IL-10 biosynthesis (Deng, 2018). In RPE, IL-10 was shown to induce apoptosis and to arrest cell proliferation (Zhao Q, 2018).

About noncoding RNAs, most of dysregulated lncRNAs were not recognized by the LncRRIsearch server. However, 4 of them (*AC011611.3, AC135048.1, AC099329.1, AC002094.1*) were predicted to regulate genes involved in inflammatory response as *MEF2A* (Xiong, 2019), *DUSP6* (Hsu, 2018), *IL18BP* (Novick, 1999), *PRKACA* (Moen,

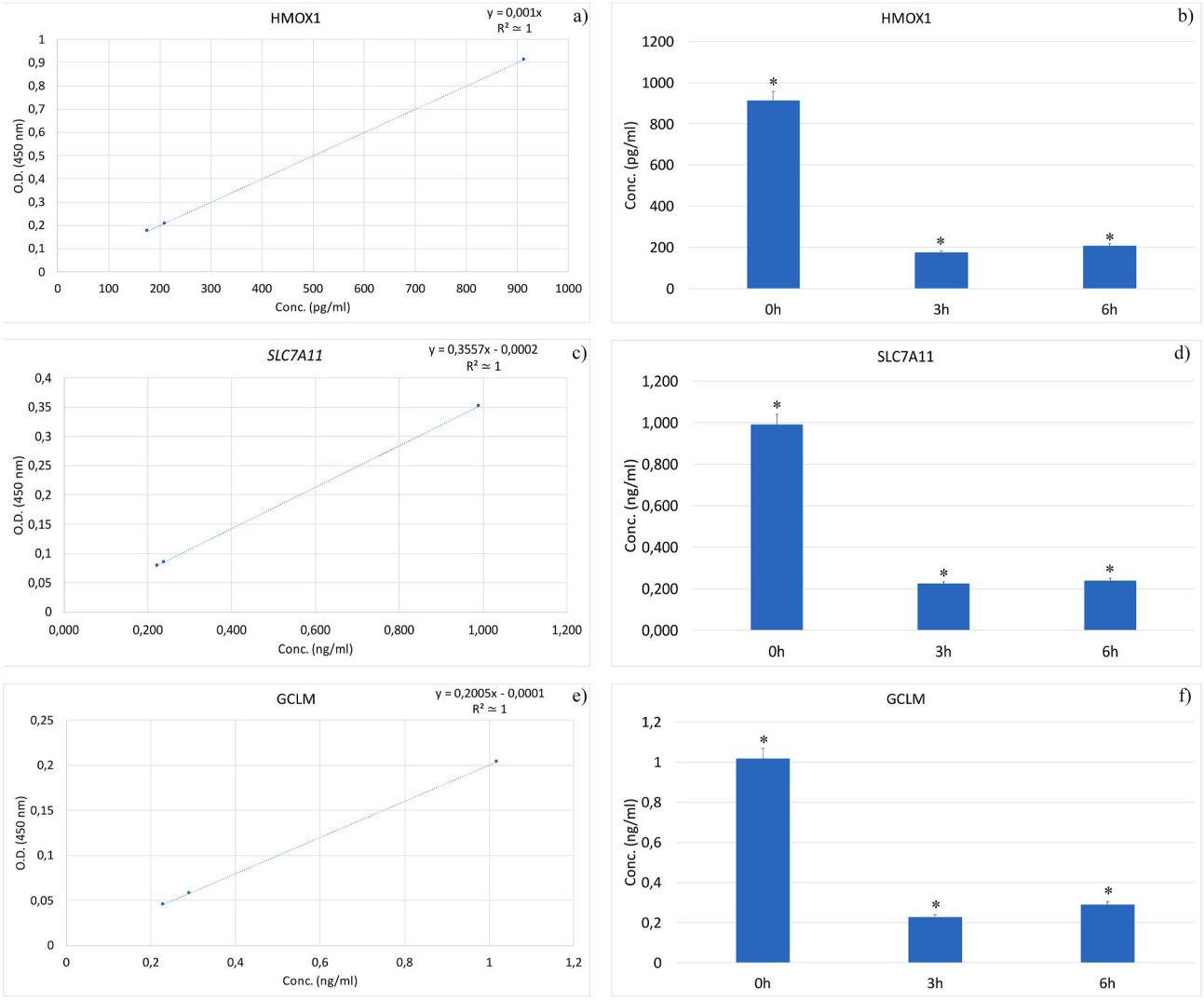

Fig. 7. Determination of ferroptosis-related proteins. Three proteins, HMOX1 (a, b), SCL7A11 (c, d) and GCLM (e, f), were quantified by ELISA assay. According to the used kits, concentration values are reported as pg/ml for HMOX1 and as ng/ml for SCL7A11 and GCLM. The three left panels (a, c, e) show linear regression correlating protein concentration with the observed absorbance at 450 nm, expressed as optical density (O.D.). The linear regression coefficient R^2 is approximated to 1. The three right panels (b, d, f) show protein concentrations at the different time points. (*): pValue < 0.05, calculated by the multiple *t*-test.

2017) and *IRS1* (Tarchick, 2019). In detail, Reactome pathway analysis clustered *MEF2A* and *DUSP6* in pathways related to IL-17 signaling and Toll-like receptors cascade. *MEF2A* encodes for a transcription factor that activates expression of stress-induced genes, under inflammatory condition (Natarajaseenivasan, 2020). *DUSP6* inhibits MAP kinases and its down-regulation enhances ERK-mediated signal transduction, enhancing gene expression of pro-inflammatory cytokines (Carson, 2017). In A2E-treated RPE cells, expression of both *MEF2A* ($\log_2$ FC = 1.029, Bonferroni-adjusted pValue = 0.0409) and *DUSP6* ($\log_2$ FC = 2.2197, Bonferroni-adjusted pValue = 0) increased, suggesting the attempt by H-RPE cells to counteract oxidative damage. Also *IL18BP* has protective role against inflammation encoding for an inhibitor of the proinflammatory cytokine IL-18 (Zhang, 2018). However, its expression did not significantly change in our samples. About *IRS1*, it is involved in IL-7 pathway (Sharfe, 1997) and its expression resulted increased in our RPE cultures, following A2E treatment. *IRS1* was shown to be chronically active in RPE under high-glucose conditions, resulting in insulin resistance (Leontieva, 2014) and photoreceptor degeneration by enhancing the biosynthesis of pro-inflammatory and pro-angiogenic molecules (Tarchick, 2019).

Globally, our results highlighted interleukin signaling triggered in RPE cells, following A2E exposure. A2E is an endogenous adduct formed by the effect of blue light on lipofuscin granules, physiologically generated during the visual cycle. A2E induces oxidative stress resulting in the activation of chronic inflammatory cascade, mediated by IL-6 and IL-1 signaling. Inflammation due to oxidative stimuli is the main cause of photoreceptor degeneration. Our results showed that under oxidative stress condition, RPE tries to rescue photoreceptor by increasing expression of anti-inflammatory cytokines, as IL-11. Being inflammatory cascade the main event that triggers photoreceptor death, a more detailed characterization of the dysregulated pathways can contribute to develop targeted therapies aimed to reduce damaging stimuli and to preserve retina functional properties.

Funding

This research did not receive any specific grant from funding agencies in the public, commercial, or not-for-profit sectors.

Accession number

According to the journal guidelines, RNA-Seq raw data were

deposited in NCBI's Sequence Read Archive (SRA) and assigned to the project identifier PRJNA622997.

Appendix A. Supplementary data

Supplementary data to this article can be found online at https://doi.org/10.1016/j.exer.2021.108641.

References

Aken, B.L., Ayling, S., Barrell, D., Clarke, L., Curwen, V., Fairley, S., Banet, J.F., Billis, K., García Girón, C., Hourlier, T., et al., 2016. The Ensembl gene annotation System. Database (Oxford). https://doi.org/10.1093/database/baw093, 2016:baw093.

Alaimo, A., Di Santo, M.C., Domínguez Rubio, A.P., Chaufan, G., García Liñares, G., Pérez, O.E., 2020. Toxic effects of A2E in human ARPE-19 cells were prevented by resveratrol: a potential nutritional bioactive for age-related macular degeneration treatment. Arch. Toxicol. 94, 553–572. https://doi.org/10.1007/s00204-019-02637-w.

Anderson, O.A., Finkelstein, A., Shima, D.T., 2013. A2E induces IL-1ß production in retinal pigment epithelial cells via the NLRP3 inflammasome. PloS One 8, e67263. https://doi.org/10.1371/journal.pone.0067263.

Bermúdez, V., Tenconi, P.E., Giusto, N.M., Mateos, M.V., 2019. Lipid signaling in retinal pigment epithelium cells exposed to inflammatory and oxidative stress conditions molecular mechanisms underlying degenerative retinal diseases. Adv. Exp. Med. Biol. 1185, 289–293. https://doi.org/10.1007/978-3-030-27378-1_47.

Bindea, G., Mlecnik, B., Hackl, H., Charoentong, P., Tosolini, M., Kirilovsky, A., Fridman, W.H., Pagès, F., Trajanoski, Z., Galon, J., 2009. ClueGO: a Cytoscape plug-in to decipher functionally grouped gene ontology and pathway annotation networks. Bioinformatics 25, 1091–1093. https://doi.org/10.1093/bioinformatics/btp101.

Bogdan, A.R., Miyazawa, M., Hashimoto, K., Tsuji, Y., 2016. Regulators of iron homeostasis: new players in metabolism, cell death, and disease. Trends Biochem. Sci. 41, 274–286. https://doi.org/10.1016/j.tibs.2015.11.012.

Bolger, A.M., Lohse, M., Usadel, B., 2014. Trimmomatic: a flexible trimmer for Illumina sequence data. Bioinformatics 30, 2114–2120. https://doi.org/10.1093/bioinformatics/btu170.

Carson, W.F. 4th, Salter-Green, S.E., Scola, M.M., Joshi, A., Gallagher, K.A., Kunkel, S.L., 2017. Enhancement of macrophage inflammatory responses by CCL2 is correlated with increased miR-9 expression and downregulation of the ERK1/2 phosphatase. Dusp6. Cell. Immunol. 314, 63–72. https://doi.org/10.1016/j.cellimm.2017.02.005.

Deng, J., James, C.H., Patel, L., Smith, A., Burnand, K.G., Rahmoune, H., Lamb, J.R., Davis, B., 2009. Human tribbles homologue 2 is expressed in unstable regions of carotid plaques and regulates macrophage IL-10 in vitro. Clin. Sci. (Lond) 116, 241–248. https://doi.org/10.1042/CS20080058.

Donato, L., D'Angelo, R., Alibrandi, S., Rinaldi, C., Sidoti, A., Scimone, C., 2020a. Effects of A2E-induced oxidative stress on retinal epithelial cells: new insights on differential gene response and retinal dystrophies. Antioxidants 9, 307. https://doi.org/10.3390/antiox9040307.

Donato, L., Scimone, C., Alibrandi, S., Nicocia, G., Rinaldi, C., Sidoti, A., D'Angelo, R., 2020b. Discovery of GLO1 new related genes and pathways by RNA-seq on A2E-stressed retinal epithelial cells could improve knowledge on retinitis pigmentosa. Antioxidants 9, 416. https://doi.org/10.3390/antiox9050416.

Fukunaga, T., Iwakiri, J., Ono, Y., Hamada, M., 2019. LncRRIsearch: a web server for lncRNA-RNA interaction prediction integrated with tissue-specific expression and subcellular localization data. Front. Genet. 10, 462. https://doi.org/10.3389/fgene.2019.00462.

Giurgiu, M., Reinhard, J., Brauner, B., Dunger-Kaltenbach, I., Fobo, G., Frishman, G., Montrone, C., Ruepp, A., 2019. CORUM: the comprehensive resource of mammalian protein complexes-2019. Nucleic Acids Res. 47 (D1), D559–D563. https://doi.org/10.1093/nar/gky973.

Heberle, H., Meirelles, G.V., da Silva, F.R., Telles, G.P., Minghim, R., 2015. InteractiVenn: a web-based tool for the analysis of sets through Venn diagrams. BMC Bioinf. 16, 169. https://doi.org/10.1186/s12859-015-0611-3.

Hsu, S.F., Lee, Y.B., Lee, Y.C., Chung, A.L., Apaya, M.K., Shyur, L.F., Cheng, C.F., Ho, F. M., Meng, T.C., 2018. Dual specificity phosphatase DUSP6 promotes endothelial inflammation through inducible expression of ICAM-1. FEBS J. 285, 1593–1610. https://doi.org/10.1111/febs.14425.

Jassal, B., Matthews, L., Viteri, G., Gong, C., Lorente, P., Fabregat, A., Sidiropoulos, K., Cook, J., Gillespie, M., Haw, R., et al., 2020. The reactome pathway knowledgebase. Nucleic Acids Res. 48 (D1), D498–D503. https://doi.org/10.1093/nar/gkz1031.

Kanehisa, M., Furumichi, M., Tanabe, M., Sato, Y., Morishima, K., 2017. KEGG: new perspectives on genomes, pathways, diseases and drugs. Nucleic Acids Res. 45 (D1), D353–D361. https://doi.org/10.1093/nar/gkw1092.

Kirchhof, B., Ryan, S.J., 1993. Differential permeance of retina and retinal pigment epithelium to water: implications for retinal adhesion. Int. Ophthalmol. 17, 19–22. https://doi.org/10.1007/BF00918862.

Kuang, F., Liu, J., Tang, D., Kang, R., 2020. Oxidative damage and antioxidant defense in ferroptosis. Front. Cell. Dev. Biol. 8, 586578 https://doi.org/10.3389/fcell.2020.586578.

Lee, J.J., Ishihara, K., Notomi, S., Efstathiou, N.E., Ueta, T., Maidana, D., Chen, X., Iesato, Y., Caligiana, A., Vavvas, D.G., 2020. Lysosome-associated membrane protein-2 deficiency increases the risk of reactive oxygen species-induced ferroptosis in retinal pigment epithelial cells. Biochem. Biophys. Res. Commun. 521, 414–419. https://doi.org/10.1016/j.bbrc.2019.10.138.

Leontieva, O.V., Demidenko, Z.N., Blagosklonny, M.V., 2014. Rapamycin reverses insulin resistance (IR) in high-glucose medium without causing IR in normoglycemic medium. Cell Death Dis. 5, e1214. https://doi.org/10.1038/cddis.2014.178.

Li, B., Ruotti, V., Stewart, R.M., Thomson, J.A., Dewey, C.N., 2010. RNA-Seq gene expression estimation with read mapping uncertainty. Bioinformatics 26, 493–500. https://doi.org/10.1093/bioinformatics/btp692.

Mitchell, A.L., Attwood, T.K., Babbitt, P.C., Blum, M., Bork, P., Bridge, A., Brown, S.D., Chang, H.Y., El-Gebali, S., Fraser, M.I., et al., 2019. InterPro in 2019: improving coverage, classification and access to protein sequence annotations. Nucleic Acids Res. 47 (D1), D351–D360. https://doi.org/10.1093/nar/gky1100.

Moen, L.V., Sener, Z., Volchenkov, R., Svarstad, A.C., Eriksen, A.M., Holen, H.L., Skålhegg, B.S., 2017. Ablation of the Cβ2 subunit of PKA in immune cells leads to increased susceptibility to systemic inflammation in mice. Eur. J. Immunol. 47, 1880–1889. https://doi.org/10.1002/eji.201646809.

Muñiz, A., Greene, W.A., Plamper, M.L., Choi, J.H., Johnson, A.J., Tsin, A.T., Wang, H.C., 2014. Retinoid uptake, processing, and secretion in human iPS-RPE support the visual cycle. Invest. Ophthalmol. Vis. Sci. 55, 198–209. https://doi.org/10.1167/iovs.13-11740.

Nagineni, C.N., Kommineni, V.K., William, A., Hooks, J.J., Detrick, B., 2010. IL-11 expression in retinal and corneal cells is regulated by interferon-gamma. Biochem. Biophys. Res. Commun. 391, 287–292. https://doi.org/10.1016/j.bbrc.2009.11.051.

Narimatsu, T., Negishi, K., Miyake, S., Hirasawa, M., Osada, H., Kurihara, T., Tsubota, K., Ozawa, Y., 2015. Blue light-induced inflammatory marker expression in the retinal pigment epithelium-choroid of mice and the protective effect of a yellow intraocular lens material in vivo. Exp. Eye Res. 132, 48–51. https://doi.org/10.1016/j.exer.2015.01.003.

Natarajaseenivasan, K., Shanmughapriya, S., Velusamy, P., Sayre, M., Garcia, A., Gomez, N.M., Langford, D., 2020. Inflammation-induced PINCH expression leads to actin depolymerization and mitochondrial mislocalization in neurons. Transl. Neurodegener. 9, 32. https://doi.org/10.1186/s40035-020-00211-4.

Novick, D., Kim, S.H., Fantuzzi, G., Reznikov, L.L., Dinarello, C.A., Rubinstein, M., 1999. Interleukin-18 binding protein: a novel modulator of the Th1 cytokine response. Immunity 10, 127–136. https://doi.org/10.1016/s1074-7613(00)80013-8.

Okonechnikov, K., Conesa, A., García-Alcalde, F., 2016. Qualimap 2: advanced multi-sample quality control for high-throughput sequencing data. Bioinformatics 32, 292–294. https://doi.org/10.1093/bioinformatics/btv566.

Orchard, S., Ammari, M., Aranda, B., Breuza, L., Briganti, L., Broackes-Carter, F., Campbell, N.H., Chavali, G., Chen, C., del-Toro, N., et al., 2014. The MIntAct project–IntAct as a common curation platform for 11 molecular interaction databases. Nucleic Acids Res. 42 (Database issue), D358–D563. https://doi.org/10.1093/nar/gkt1115.

Parmar, V.M., Parmar, T., Arai, E., Perusek, L., Maeda, A., 2018. A2E-associated cell death and inflammation in retinal pigmented epithelial cells from human induced pluripotent stem cells. Stem Cell Res. 27, 95–104. https://doi.org/10.1016/j.scr.2018.01.014.

Ritchie, M.E., Phipson, B., Wu, D., Hu, Y., Law, C.W., Shi, W., Smyth, G.K., 2015. Limma powers differential expression analyses for RNA-sequencing and microarray studies. Nucleic Acids Res. 43, e47. https://doi.org/10.1093/nar/gkv007.

Rutar, M., Natoli, R., Chia, R.X., Valter, K., Provis, J.M., 2015. Chemokine-mediated inflammation in the degenerating retina is coordinated by Müller cells, activated microglia, and retinal pigment epithelium. J. Neuroinflammation 12, 8. https://doi.org/10.1186/s12974-014-0224-1.

Sharfe, N., Roifman, C.M., 1997. Differential association of phosphatidylinositol 3-kinase with insulin receptor substrate (IRS)-1 and IRS-2 in human thymocytes in response to IL-7. J. Immunol. 159, 1107–1114.

Somasundaran, S., Constable, I.J., Mellough, C.B., Carvalho, L.S., 2020. Retinal pigment epithelium and age-related macular degeneration: a review of major disease mechanisms. Clin. Exp. Ophthalmol. Online ahead of print. https://doi.org/10.1111/ceo.13834.

Strait, S., Loman, R., Erickson, L., DeBenedictis, M., 2020. Inherited retinal degeneration current genetics practices - a needs assessment. Ophthalmic Genet. 1–6. https://doi.org/10.1080/13816810.2020.1804943.

Sun, Y., Zheng, Y., Wang, C., Liu, Y., 2018. Glutathione depletion induces ferroptosis, autophagy, and premature cell senescence in retinal pigment epithelial cells. Cell Death Dis. 753 https://doi.org/10.1038/s41419-018-0794-4.

Tarchick, M.J., Cutler, A.H., Trobenter, T.D., Kozlowski, M.R., Makowski, E.R., Holoman, N., Shao, J., Shen, B., Anand-Apte, B., Samuels, I.S., 2019. Endogenous insulin signaling in the RPE contributes to the maintenance of rod photoreceptor function in diabetes. Exp. Eye Res. 180, 63–74. https://doi.org/10.1016/j.exer.2018.11.020.

The Gene Ontology Consortium, 2017. Expansion of the gene ontology knowledgebase and resources. Nucleic Acids Res. 45 (D1), D331–D338. https://doi.org/10.1093/nar/gkw1108.

The UniProt Consortium, 2018. UniProt: the universal protein knowledgebase. Nucleic Acids Res. 46, 2699. https://doi.org/10.1093/nar/gky092.

Uhlen, M., Zhang, C., Lee, S., Sjöstedt, E., Fagerberg, L., Bidkhori, G., Benfeitas, R., Arif, M., Liu, Z., Edfors, F., et al., 2017. A pathology Atlas of the human cancer transcriptome. Science 357, eaan2507. https://doi.org/10.1126/science.aan2507.

Wain, H.M., Bruford, E.A., Lovering, R.C., Lush, M.J., Wright, M.W., Povey, S., 2002. Guidelines for human gene nomenclature. Genomics 79, 464–470. https://doi.org/10.1006/geno.2002.6748.

Wang, J., Feng, Y., Han, P., Wang, F., Luo, X., Liang, J., Sun, X., Ye, J., Lu, Y., Sun, X., 2018. Photosensitization of A2E triggers telomere dysfunction and accelerates

retinal pigment epithelium senescence. Cell Death Dis. 9, 178. https://doi.org/10.1038/s41419-017-0200-7.

Wooff, Y., Fernando, N., Wong, J.H.C., Dietrich, C., Aggio-Bruce, R., Chu-Tan, J.A., Robertson, A.A.B., Doyle, S.L., Man, S.M., Natoli, R., 2020. Caspase-1-dependent inflammasomes mediate photoreceptor cell death in photo-oxidative damage-induced retinal degeneration. Sci. Rep. 10, 2263. https://doi.org/10.1038/s41598-020-58849-z.

Xiong, Y., Wang, L., Jiang, W., Pang, L., Liu, W., Li, A., Zhong, Y., Ou, W., Liu, B., Liu, S. M., 2019. MEF2A alters the proliferation, inflammation-related gene expression profiles and its silencing induces cellular senescence in human coronary endothelial cells. BMC Mol. Biol. 20, 8. https://doi.org/10.1186/s12867-019-0125-z.

Zhang, L.M., Zhang, J., Zhang, Y., Wang, L., Fei, C., Yi, Z.W., Dong, L., 2018. Interleukin-18 binding protein attenuates lipopolysaccharide-induced acute lung injury in mice via suppression NF-κB and activation Nrf2 pathway. Biochem. Biophys. Res. Commun. 505, 837–842. https://doi.org/10.1016/j.bbrc.2018.09.193.

Zhao, M., Liu, Y., Liu, R., Qi, J., Hou, Y., Chang, J., Ren, L., 2018. Upregulation of IL-11, an IL-6 family cytokine, promotes tumor progression and correlates with poor prognosis in non-small cell lung cancer. Cell. Physiol. Biochem. 45, 2213–2224. https://doi.org/10.1159/000488166.

Zhao, Q., Ji, M., Wang, X., 2018. IL-10 inhibits retinal pigment epithelium cell proliferation and migration through regulation of VEGF in rhegmatogenous retinal detachment. Mol. Med. Rep. 17, 7301–7306. https://doi.org/10.3892/mmr.2018.8787.

Zhuang, Z., Pan, X., Zhao, K., Gao, W., Liu, J., Deng, T., Qin, W., 2019. The effect of interleukin-6 (IL-6), interleukin-11 (IL-11), signal transducer and activator of transcription 3 (STAT3), and AKT signaling on adipocyte proliferation in a rat model of polycystic ovary syndrome. Med. Sci. Mon. Int. Med. J. Exp. Clin. Res. 25, 7218–7227. https://doi.org/10.12659/MSM.916385.